

Deep learning-assisted common temperature measurement based on visible light imaging

Jia-Yi Zhu(朱佳仪), Zhi-Min He(何志民), Cheng Huang(黄成), Jun Zeng(曾峻), Hui-Chuan Lin(林惠川), Fu-Chang Chen(陈福昌), Chao-Qun Yu(余超群), Yan Li(李燕), Yong-Tao Zhang(张永涛), Huan-Ting Chen(陈焕庭), and Ji-Xiong Pu(蒲继雄)

Citation: Chin. Phys. B, 2024, 33 (**8**): 080701. DOI: 10.1088/1674-1056/ad4cd9

What follows is a list of articles you may be interested in

Anti-Stokes/Stokes temperature calibration and its application in laser-heating diamond anvil cells

Minmin Zhao(赵旻旻), Binbin Wu(吴彬彬), Jingyi Liu(刘静仪), and Li Lei(雷力)

Chin. Phys. B, 2023, 32 (**9**): 090704. DOI: 10.1088/1674-1056/accd55

Learnable three-dimensional Gabor convolutional network with global affinity attention for hyperspectral image classification

Hai-Zhu Pan(潘海珠), Mo-Qi Liu(刘沫岐), Hai-Miao Ge(葛海淼), and Qi Yuan(袁琪)

Chin. Phys. B, 2022, 31 (**12**): 120701. DOI: 10.1088/1674-1056/ac8cd7

High-precision nuclear magnetic resonance probe suitable for *in situ* studies of high-temperature metallic melts

Ao Li(李傲), Wei Xu(许巍), Xiao Chen(陈霄), Bing-Nan Yao(姚冰楠), Jun-Tao Huo(霍军涛), Jun-Qiang Wang(王军强), and Run-Wei Li(李润伟)

Chin. Phys. B, 2022, 31 (**4**): 040706. DOI: 10.1088/1674-1056/ac4a70

Cascaded dual-channel fiber SPR temperature sensor based on liquid and solid encapsulations

Yong Wei(魏勇), Lingling Li(李玲玲), Chunlan Liu(刘春兰), Jiangxi Hu(胡江西), Yudong Su(苏于东), Ping Wu(吴萍), and Xiaoling Zhao(赵晓玲)

Chin. Phys. B, 2021, 30 (**10**): 100701. DOI: 10.1088/1674-1056/ac0426

An artificial synapse by superlattice-like phase-change material for low-power brain-inspired computing

Qing Hu(胡庆), Boyi Dong(董博义), Lun Wang(王伦), Enming Huang(黄恩铭), Hao Tong(童浩), Yuhui He(何毓辉), Ming Xu(徐明), Xiangshui Miao(缪向水)

Chin. Phys. B, 2020, 29 (**7**): 070701. DOI: 10.1088/1674-1056/ab892a

---

Deep learning-assisted common temperature measurement based on visible light imaging

Jia-Yi Zhu(朱佳仪)[1], Zhi-Min He(何志民)[1], Cheng Huang(黄成)[1], Jun Zeng(曾峻)[1], Hui-Chuan Lin(林惠川)[1,†], Fu-Chang Chen(陈福昌)[1], Chao-Qun Yu(余超群)[1], Yan Li(李燕)[1], Yong-Tao Zhang(张永涛)[1], Huan-Ting Chen(陈焕庭)[1], and Ji-Xiong Pu(蒲继雄)[1,2]

[1] *College of Physics and Information Engineering, Minnan Normal University, Zhangzhou* 363000, *China*

[2] *Fujian Provincial Key Laboratory of Light Propagation and Transformation, College of Information Science & Engineering, Huaqiao University, Xiamen* 361021, *China*

(Received 2 April 2024; revised manuscript received 26 April 2024; accepted manuscript online 17 May 2024)

Real-time, contact-free temperature monitoring of low to medium range (30 °C–150 °C) has been extensively used in industry and agriculture, which is usually realized by costly infrared temperature detection methods. This paper proposes an alternative approach of extracting temperature information in real time from the visible light images of the monitoring target using a convolutional neural network (CNN). A mean-square error of < 1.119 °C was reached in the temperature measurements of low to medium range using the CNN and the visible light images. Imaging angle and imaging distance do not affect the temperature detection using visible optical images by the CNN. Moreover, the CNN has a certain illuminance generalization ability capable of detection temperature information from the images which were collected under different illuminance and were not used for training. Compared to the conventional machine learning algorithms mentioned in the recent literatures, this real-time, contact-free temperature measurement approach that does not require any further image processing operations facilitates temperature monitoring applications in the industrial and civil fields.

Keywords: convolutional neural network, visible light image, temperature measurement, low-to-medium-range temperatures

PACS: 07.05.Mh, 07.07.Df, 78.20.Ci **DOI:** 10.1088/1674-1056/ad4cd9

1. Introduction

Measurement of common temperatures (30 °C–150 °C) that are closely related to human activities is in great demand in a wide range of industrial, agricultural, civil, and medical applications.[1–3] Typically, common temperature objects radiate heat outwards in the form of infrared electromagnetic waves at infrared wavelengths (6 μm–13 μm), which are not detectable by the sensors of cameras developed for visible light imaging. Thus, a widely used, non-contact method of common temperature measurement is infrared thermometry using infrared sensors.[4] Despite the fact that infrared thermometry is now very well developed, high cost in hardware becomes a barrier to its widespread use.[5] Nowadays, surveillance cameras are present in all corners of this world, especially in the industrial fields such as power grids. On condition that these cameras could also be used to monitor the temperature of certain objects in front of the cameras in real time, it will be great significance for the operation and maintenance of places such as substations. The visible light that illuminates an object of temperature of low to medium range is reflected from it and modulated by its temperature simultaneously.[6] Thus, the light reflected by an object actually contains temperature information of object itself. If the temperature information can be extracted from the visible light reflected from the object that captured by the sensors of surveillance cameras, the monitoring of low-to-medium-range temperatures by using visible optical image can be realized. This method is known as thermoreflectance imaging technology, which can be traced back to the 1960s. However, because there is no simple linear relationship between reflectivity and temperature, it is still a great challenge for the realization of temperature monitoring by the thermoreflectance visible imaging technology.[7–12] Recently, with the rise of machine learning techniques, researchers have made efforts to apply machine learning to visible light thermometry of metal surfaces of low to medium temperature range. Such as, a prediction model describing the connection between image features and temperature was proposed by Wang *et al.*, and it was combined with Retinex theory to improve the accuracy;[13] Li *et al.* proposed a full-wavelength multi-incidence angle thermally modulated light reflection temperature measurement mechanism based on visible images, and an error of 0.7 °C was achieved with images of RAW format as the optimizing data;[6] Du reported the visible light thermometry in sunlight conditions using machine learning, resulting in errors of below 2.8 °C for aluminum alloy wire clamps, 3.9 °C for copper tinned wire rows and 2.87 °C for copper wire rows;[14] Nie *et al.* proposed a similar machine learning approach in sunlight environment while using videos from surveillance camera as the data for temperature

†Corresponding author. E-mail: lhc1810@mnnu.edu.cn

© 2024 Chinese Physical Society and IOP Publishing Ltd

information extraction.[15] These works stated above all employed the same machine learning algorithm, k-nearest neighbor algorithm (KNN). The KNN approach involves a tedious operation procedure of labeling the input data, classifying data through human perception and finally training the predictive model to build the connection between the input data and the labels. In such a procedure, significant human intervention of recognizing key features for classification is required and the final accuracy also highly relies on the researchers' sophistication of classification.[16,17] Compared with machine learning, deep learning learns without human intervention and allows for a deeper, more abstract description of the properties and features of objects.[18] With its powerful learning capabilities, deep learning has been used extensively in recent years in image processing applications.[19–21] In order to realize visible light thermometry conveniently, the exploration of extracting temperature information from visible optical images utilizing deep learning would be a very meaningful work. Therefore, the visible light thermometry utilizing deep learning has been study in this paper, hoping to realize the target temperature measurement by using the images collected by security cameras. In the subsequent sections of this paper, the theoretical analysis, experimental process, and detection results for common temperature measurement by using the CNN will be discussed in detail.

2. Theoretical analysis of the CNN for common temperature measurement

Reflected light from the surface of the target object can be derived from the Fresnel equation, which is a complex function of the general refractive index, extinction coefficient, and angle of incidence. The spectral flux that reflected from the surface of the target object received by the camera can be expressed as

$$\Phi_{\mathrm{im}}(\lambda) = D\big[AF(n,k,\theta)I_{\mathrm{i}}(\lambda)+BF(n,k,\theta)I_{\mathrm{i}}(\lambda) +CF(n,k,\theta)I_{\mathrm{i}}(\lambda)\big], \tag{1}$$

where $F(n,k,\theta)$ is the Fresnel reflectance, n is the refractive index, k and θ are the extinction coefficient and the incident angle respectively. $I_{\mathrm{i}}(\lambda)$ and $\Phi_{\mathrm{im}}(\lambda)$ in Eq. (1) are the intensity of incident light and the value of illumination received by each pixel of the CCD camera. A, B, and C are the constants determined by the surface roughness of the object, the inherent structural parameters of the camera and the position of the camera relative to the observed surface. Since the general refractive index and extinction coefficient are the functions of wavelength and temperature of the target object, the Fresnel reflectance is also a function of wavelength and temperature.[6] According to Eq. (1), the refractive index of the target object changes with its temperature, which alters the illuminance received by each pixel of the camera. Moreover, the illumination values of the red, green, and blue channels for each pixel of a color camera are

$$R = \int V_{\mathrm{r}}(\lambda)\,\Phi_{\mathrm{im}}(\lambda)\,\mathrm{d}\lambda, \tag{2}$$

$$G = \int V_{\mathrm{g}}(\lambda)\,\Phi_{\mathrm{im}}(\lambda)\,\mathrm{d}\lambda, \tag{3}$$

$$B = \int V_{\mathrm{b}}(\lambda)\,\Phi_{\mathrm{im}}(\lambda)\,\mathrm{d}\lambda, \tag{4}$$

where $V_{\mathrm{r}}(\lambda)$, $V_{\mathrm{g}}(\lambda)$, and $V_{\mathrm{b}}(\lambda)$ are the spectral response functions for red, green, and blue channels. Obviously, the temperature of the target object not only affects the grayscale illuminance of each pixel, but also affects the distribution of illuminance in different color channels of a color image. Therefore, temperature detection of the target object through visible light optical images is feasible if temperature features can be extracted and calibrated from images of different target temperatures in advance.

In order to obtain visible light optical images for temperature information extraction and calibration, a copper sheet, which was taken as target object, attached on a hotplate was employed as the target for temperature detection, as shown in Fig. 1. The hotplate is a stainless-steel electric heating plate of model type DB-1 with temperature range from room temperature to 300 °C and temperature control accuracy of 0.1 °C. The thermocouple sensor of a thermometer was attached on the copper sheet to monitor its real-time temperature. The Pike F-421B camera with 2048×2048 resolution and 16-bit TIFF output image formation was used to take the pictures of the target at different temperatures. One LED light with adjustable brightness was placed above the target as the illumination light source. The temperature of the hotplate was adjusted upward in steps of 5 °C and 200 images of the target were taken for each temperature step. A data set including 2600 images was then constructed for the temperature range from 30 °C to 90 °C.

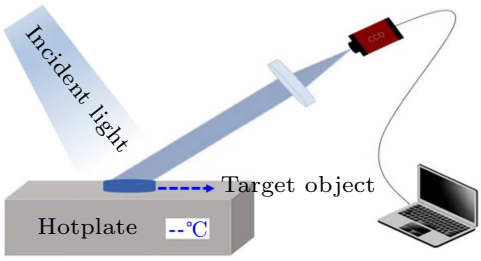


Fig. 1. Optical imaging diagram in the laboratory.

A convolutional neural network (CNN) is used for target temperature detection of the copper sheet from the acquired image data set. In order for the network to recognize target features at different temperatures to determine the current temperature of the target, the network should be first trained with appropriate data set. The pre-prepared data set of target images at different temperatures was divided into three portions

of the training set, the validation set, and the test set, the exact numbers of which are 2080, 560, and 280, respectively. Each image in the data sets was cropped to 150×150 pixels to maximize target retention and remove unwanted background. The structure of the CNN network is shown in Fig. 2. It is composed of four parts: input layer (Input), convolutional layer (Conv), pooling layer (Pooling), and fully connected layer (FC). The input layer is a matrix of 150×150 in size that is identical to the pixel size of the images in the data sets. The convolutional layer is the core of the network and performs convolution operations to extract image features, which is done by converting the image into a matrix using a 3×3 convolution kernel sliding from the top left corner and whose result is a 3×3 output matrix. For RGB color images, the convolution results of three channels are summed up to form the output. There are three convolutional layers in the network with the number of convolutional kernels of 512, 256, and 128 respectively and the step size of 1. Maximum pooling is used in the pooling layer, for which the maximum value is selected from the neighboring regions as a representative of that region to reduce the amount of computation and prevent overfitting. A maximum pooling layer of size (2, 2) is used behind each convolutional layer in the model. Neurons in the fully connected layer are associated with each position in the convolutional layer, compressing the features into vectors to facilitate classification by the classifier. The number of neurons in each layer is gradually reduced through a series of dense layers and ReLU is used as the activation function. In the final layer, a single neuron is employed for regression task, the output value of which represents the predicted value of the target variable. In addition, the CNN model in this paper was trained with the batch size of 20 and the learning rate of 0.0002. The mean squared error (MSE) and Adam algorithm were used as the loss function and the optimization algorithm for the model, respectively.

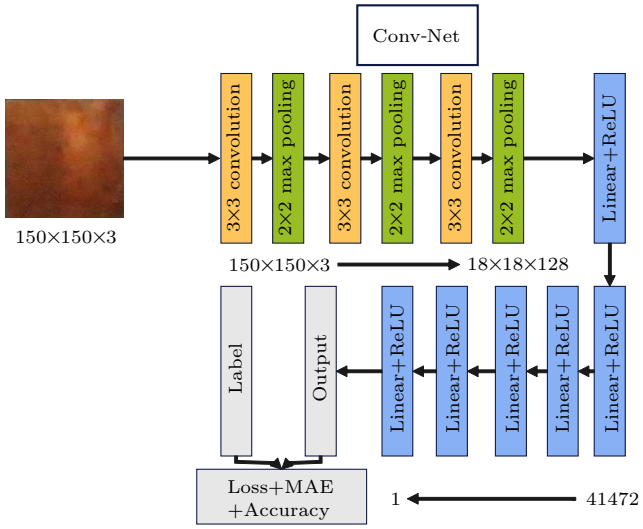


Fig. 2. Network structure of the CNN.

After 20 epochs of training, the images of the test set were fed to the CNN which output the predicted temperatures based on the image features. The predicted temperatures were used to compare with the actual temperatures corresponding to the images as a way to verify the accuracy of temperature detection by the CNN. The verification results are shown in Fig. 3. It can be found obviously that the predicted temperatures are in good agreement with the actual temperatures and the trained CNN can accurately achieve the temperature of the target from its visible optical images. Figure 3 shows reducing the illumination from 600 lux to 400 lux does not increase the prediction error that is $< \pm 2$ °C for both cases. This result shows that the temperature information of a target can be detected from its visible light images by using the CNN, that is, the method based on deep learning can be used for the detection of common temperatures through visible light images.

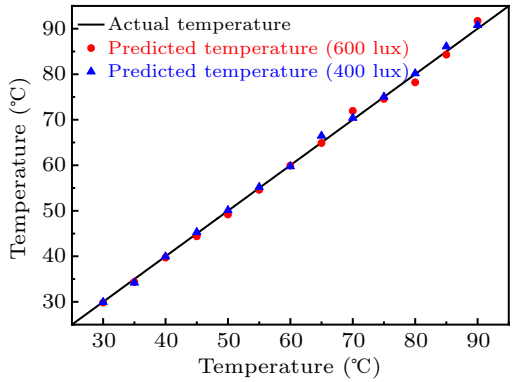


Fig. 3. Temperature detection by the CNN under different illuminances.

3. Temperature detection by CNN in sunlight environment

In many applications, temperature detection is performed outdoors, and the reflected light from target object comes from sunlight. In order to investigate whether this visible light temperature detection approach by using the CNN is applicable to outdoor temperature detection, the experiment mentioned above was moved to an outdoor environment to collect the images of data sets and the experimental setup is indicated Fig. 4. Copper sheet attached onto the hotplate was still employed as the target of temperature detection, as shown in inset (b) of Fig. 4. The thermometer with its thermocouple sensor attached onto the copper sheet indicating the accurate temperature of the target. A spectral color illuminance meter (SPIC-200) was used to monitor the color temperature and illuminance of the ambient light, as shown in insets (a) and (d) of Fig. 4. The SPIC-200 meter measures the illuminance ranging from 0.1 lux to 200 klux with an accuracy of ±(3% reading +1). A Canon EOS 200D II camera was used to capture a video of the target and then still images of 8-bit JPG formation were extracted from the video. The reason for having the camera take video instead of photos is that, in some real-world

applications, surveillance cameras that take video are used to fulfill the job of visible light temperature detection and this experiment was designed to simulate a real-world application scenario. The target was first heated to a certain temperature by the hot plate, then the hot plate was turned off and the target cooled naturally while the camera started recording video. The recording process lasted about 30 min, during which the target temperature dropped from 130 °C to around 45 °C. A total of 4.6×10^4 frames within the 30-min acquisition period. A total of 4.6×10^4 frames were extracted from this 30-min video and categorized according to the actual temperature of the target at each frame. They were then divided into a training set, a test set and a validation set. The camera's imaging angle and imaging distance may affect the accuracy of temperature detection, so a series of experiments with different imaging angles and imaging distances were carried out and 4.6×10^4 images were obtained for each experiment.

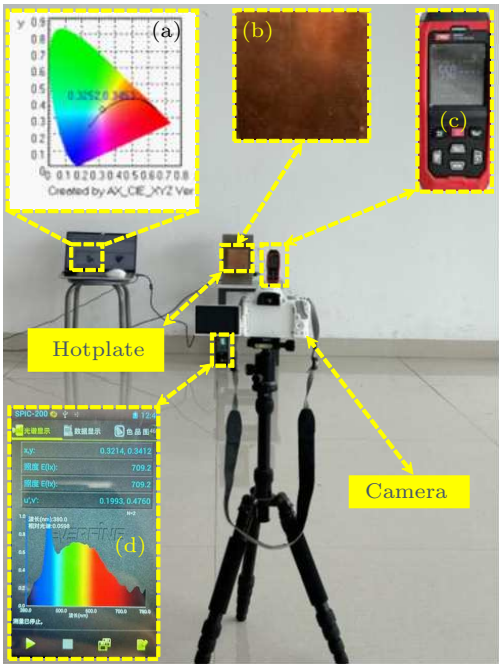


Fig. 4. Experimental setup for temperature detection in outdoor environment.

An epoch in the network training process refers to a single pass through the entire training set, which is used to determine when to stop training. After each epoch, the accuracy for the CNN trained with images of the training set are calculated and plotted in Fig. 5. Apparently, with the increase of epochs the detection accuracy of CNN is gradually increased. However, the accuracy of CNN via training epoch for different imaging distances is different. The closer the imaging distance, the higher the detection accuracy, and the optimal accuracy was obtained for the imaging distance of 2 m. This may be attributed to the fact that the image of closer imaging distance contains clearer and richer details of the target, which help the model learn the target temperature information better. Similarly, the curve for the imaging distance of 6 m shows the worst accuracy due to the loss of target details in the images, which make it difficult for the model to capture subtle changes in the target temperature.

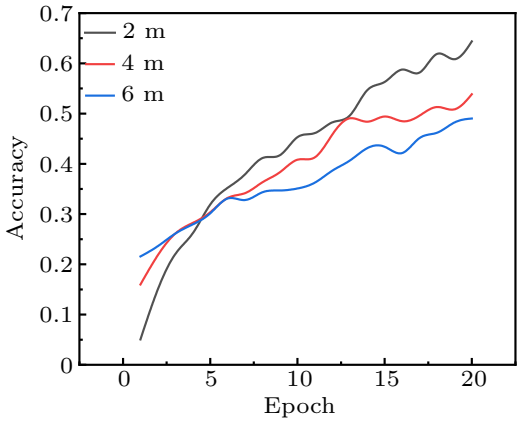


Fig. 5. Accuracy derived from training at different distances.

After the training was completed, the images in the test set were used to verify the performance of this CNN on temperature detection. For the experiments in which the camera was located directly in front of the target, the results are illustrated in Fig. 6, in which panels (a), (b), and (c) are the experimental results for the imaging distances of 2 m, 4 m, and 6 m, respectively. As it can be seen from Fig. 6, the trained CNN is able to detect the target temperatures from the visible images effectively under all three imaging distance conditions. To quantify the accuracy of detection, mean absolute error (MAE) between the predicted temperatures and the actual temperatures was calculated using Eq. (5) where n is the number of samples, represents the actual temperature and represents the predicted temperature. The MAEs corresponding to the imaging distances of 2 m, 4 m, and 6 m are 1.119 °C, 1.366 °C, and 2.897 °C, respectively. By comparing the three MAEs it can be concluded that the detection error of the CNN increases with the increase of the imaging distance. This result can be attributed to the loss of reflected light signal, because with the increase of imaging distance the monitoring object occupying fewer pixels on the imaging surface. This can be attributed to the loss of reflected light signal. As the imaging distance increases, the pixel size occupied by the target in the image becomes smaller. Therefore, the target image contains less temperature information and the temperature detection becomes more difficult.

$$\mathrm{MAE} = \left(\frac{1}{n}\right) \sum_i^n |y_i - x_i|, \tag{5}$$

As it can be shown in Eq. (1), background illuminance is an important parameter that affects the performance of temperature detection using visible optical images. In the aforementioned outdoor temperature detection experiments, target image collections were performed in an outdoor environment

without active lighting, in which the real-time ambient illuminance was also recorded simultaneously. As shown in the experimental setup of Fig. 4, an SPIC-200 spectral color illuminance meter was utilized to measure the ambient illuminance value. The variations of measured illuminance over time during aforementioned experiments are depicted in Fig. 7(a). As it can be seen from Fig. 7(a), the background illuminance fluctuated during the video recording processes, *i.e.*, while the target was experiencing temperature changes. Among the illuminance curves in Fig. 7(a), the greatest variation in ambient illuminance is observed for the experiment with an imaging distance of 4 m, which varies from 400 lux to 1300 lux. However, from the results in Fig. 6, such a huge change in background illumination in this experiment did not result in a substantial increase in detection error. For the temperature detection experiment with an imaging distance of 6 m, the background illuminance varied only from 350 lux to 600 lux during the image collection process. The MAE of 1.366 °C for temperature detection at 4-m imaging distance is much smaller than the MAE of 2.897 °C for temperature detection at 6-m imaging distance. This suggests that an appropriately trained CNN can detect temperature information from a visible light image even if this image is captured under different illuminance.

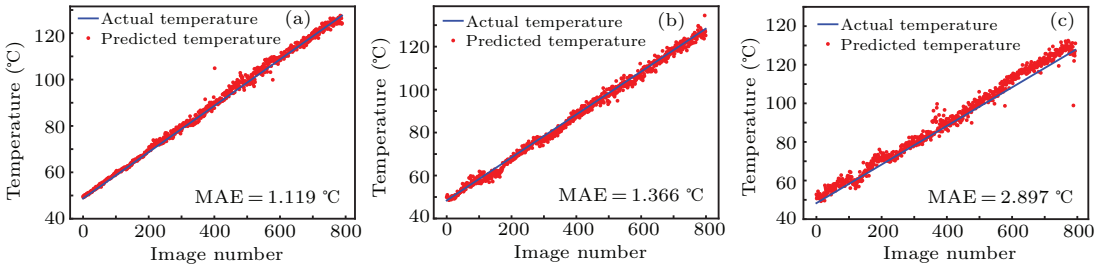


Fig. 6. Temperature detection results for experimental setups of different imaging distances: (a) 2 m, (b) 4 m, and (c) 6 m.

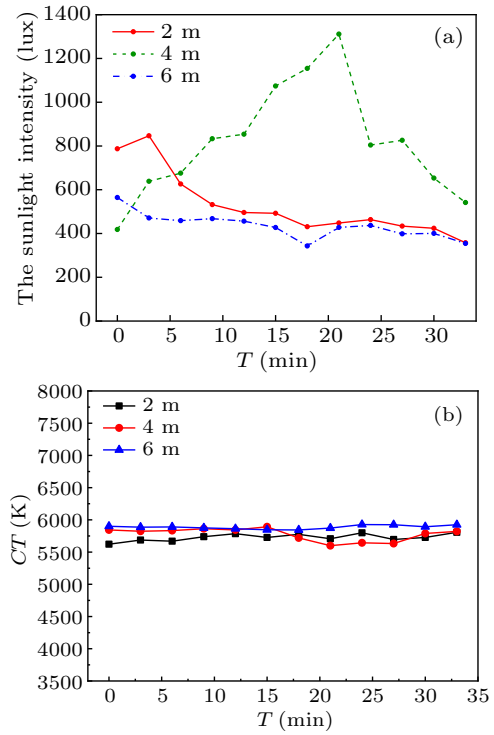


Fig. 7. Variations of sunlight intensity and color temperature of ambient light over time during target video recording, (a) sunlight intensity, (b) color temperature of ambient light.

In addition to the illuminance value of the ambient light, its color temperature was also recorded by the SPIC-200 spectral color illuminance meter. Figure 7(b) indicates the color temperature of the background light changed over time during target video recording process. It can be seen that ambient light also changed in its color temperature in addition to changes in illuminance. As known that alterations in the incident light's color temperature lead to changes in deep semantic chromatic features (DSCFs) of the target image, such as pixel mean, polar deviation, and standard deviation. As a result, variation in color temperature may interfere with the target temperature information embedded in the image, thus affecting the temperature information extraction and temperature detection by the CNN. From the results indicated in Fig. 7(b), the trained CNN can still detect temperature information from a visible light image even if this image is captured under different color temperatures.

In real application scenarios, the target to be measured in temperature is not necessarily located directly in front of the camera, but more often than not, is imaged at an angle from the side. Different imaging angles may change the gray scale distribution and DSCFs of the target in the image. Thus the effect of the imaging angle on the accuracy of the visible light temperature detection approach by using the CNN needs to be considered. In the next experimental setups, the distance between the camera and the target was kept at 2 m, and the camera position was adjusted so that the angle between the camera optical axis and the target normal was 15°, 30°, and 45°, respectively. For these three experimental setups, the experimental procedure was consistent with the previous ones, in which the target was captured on video during heated up and the target images were extracted from the video to form the data sets for the CNN training and validation. The results are plotted in Fig. 8. Figure 8(a) shows the experimental results for the camera located at 2 m directly in front of the target, *i.e.*, the imaging angle of 0°. Figures 8(b)–8(d) are the results for the imaging angles of 15°, 30°, and 45°, respectively. It can be

concluded from the figures that the CNN is able to detect the target temperature accurately in all four imaging angle occasions while different detection accuracies were achieved. The MAEs were calculated as 1.119 °C for imaging angle of 0°, 2.877 °C for 15°, 3.391 °C for 30° and 3.101 °C for 45°. The results show that the trained CNN can still detect temperature information from a visible light image even if the target is not frontally recorded in the image.

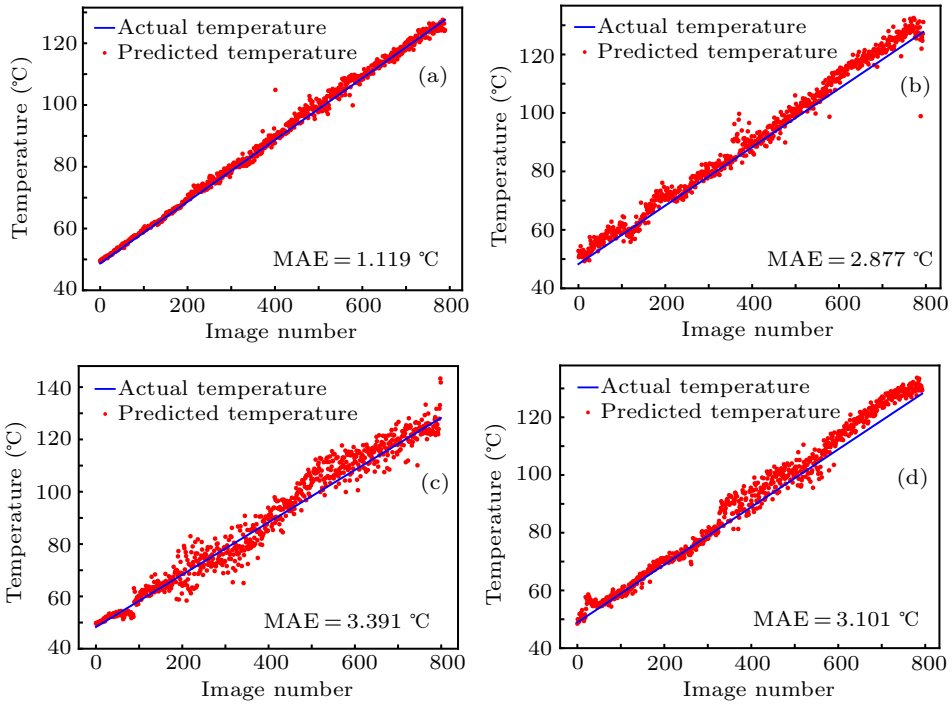


Fig. 8. Temperature detection results for experimental setups of different imaging angles with imaging distance of 2 m, (a) 0°, (b) 15°, (c) 30°, and (d) 45°.

In a realistic deep learning application, the network must have been trained with priori data collected at some time in the past before being applied to temperature detections at another time. As mentioned earlier, outdoor lighting conditions are exceptionally complex, illuminance in particular changing all the time. The priori dataset could not cover all outdoor lighting conditions generally. It is most likely that the outdoor lighting condition under which the current target image was taken is not the same as that of any of the images in the priori dataset. In this case, is the CNN still able to detect the target temperature accurately? A strategy of misaligned training and validation of the CNN is used to probe this question. In this strategy, the CNN is trained with an image data set at a certain illumination level and validated with an image dataset at another illumination level. Since outdoor illuminance cannot be controlled, multiple image collection experiments were carried out and images of specific background illuminance were selected to form the data sets. A total of four datasets were constructed. Images with background illuminance of 400 lux and 700 lux were combined to form a training set. One validation set consists of images with background illuminance of 450 lux and the other consists of images with that of 500 lux. The network was trained by the training set and validated by two validation sets respectively. The validation results are shown in Fig. 9, in which panel (a) is the result for the validation set of 450 lux, and panel (b) is for the validation set of 500 lux. Even though the images in the validation set were taken under completely different illuminances than those in the training set, the trained CNN was still able to correctly detect the target temperatures. By comparing Fig. 9(a) and Fig. 9(b), the CNN shows significantly better performance in temperature detection for images of 450 lux than for those of 500 lux. The former has an MAE of 3.792 °C and the latter has an MAE of 7.935 °C. Also, in Fig. 9(b), the predicted temperature values are generally smaller than the corresponding actual values. These are due to the fact that the illuminance of 450 lux is closer to the images' background illuminance of 400 lux in the training set than that of 500 lux. This proves that the CNN has a certain generalization ability of illuminance in common temperature measurement based on visible light image. Although the illumination under which the target was imaged is different from but close to that of any image in the training set, the CNN can still detect temperature information from the visible light image.

In summary, the error of temperature detection based on the CNN and visible light images is increased if the images used for temperature detection are taken under different background illumination or imaging conditions than the images used for the training of the CNN. Therefore, in order to minimize the error, the background illumination and other imaging conditions need to be strictly controlled to be consistent with those of the images in the training set in temperature detection

based on the CNN and visible light images.

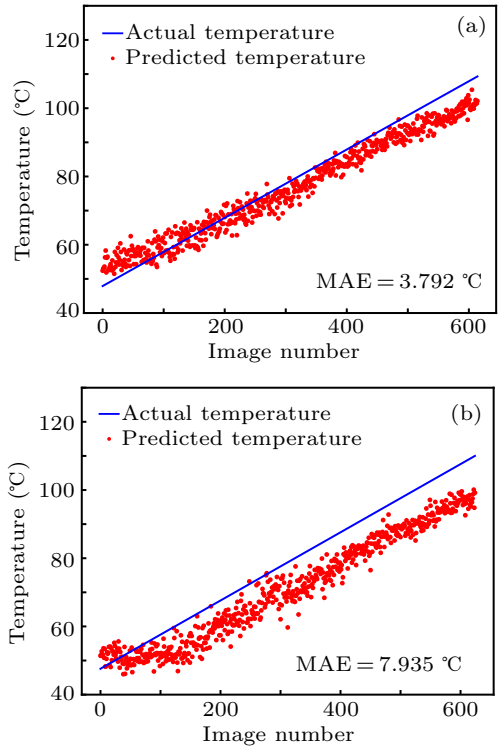


Fig. 9. Temperature detection of CNN by untrained visible light image, illuminations of (a) 450 lux and (b) 500 lux.

4. Conclusion

The use of visible light images to detect common temperatures has considerable application value. Assisted with the convolutional neural network (CNN), detection of temperature ranging from 45 °C to 130 °C has been realized in this paper. Under experimental setups with different imaging angles and imaging distances, visible light images of a target were collected and used for network training and validation. The results show that, after the network being appropriately trained, imaging angle and imaging distance do not affect the temperature detection using visible light images by the CNN. Moreover, the CNN trained by images collected under a certain illumination level can accurately detect temperatures through the images taken under another illumination level. It suggests that the CNN has a generalization ability of illuminance capable of generalizing regularities from limited known data in the training set and applying them to unknown situations. This temperature detection approach using visible light images and deep learning technology will have important applications in industry and agriculture. Note that the deviation of background illumination or other imaging conditions would have an impact on the detection results, while it is difficult to strictly control the imaging conditions to match those of the images in the training set in practice, especially in outdoor temperature detection applications. In order to avoid the effect of the deviation of imaging conditions on temperature detection and to improve its accuracy, some algorithms that can extract the reflective component from an image can be used to process the target images.

Acknowledgements

Project supported by the National Natural Science Foundation of China (Grant Nos. 61975072 and 12174173) and the Natural Science Foundation of Fujian Province, China (Grant Nos. 2022H0023, 2022J02047, ZZ2023J20, and 2022G02006).

References

[1] Li B J 2007 *Study on the relationship between land use and ecological environment*, Ph.D Dissertation (Nanjing: Nanjing Agricultural University) (in Chinese)
[2] Guo F 2016 *Chemical Engineering Management* **29** 269 (in Chinese)
[3] Zhang H R 2022 *Fault diagnosis and health assessment of power transformers based on data information mining*, M.S. Thesis (Jinan: Shandong University) (in Chinese)
[4] Li T F 2020 *High Voltage Apparatus* **56** 246 (in Chinese)
[5] Zhao H 2015 *Science and Technology Wind* **262** 118 (in Chinese)
[6] Li W M 2021 *Research on the mechanism and method optimization of artificial intelligence temperature measurement based on visible light images*, M.S. Thesis (Wuhan: Huazhong University of Science and Technology) (in Chinese)
[7] Houchens A F and Hering R G 1967 *Houchens A F and Hering R G 1967 Proceedings of 2nd Thermophysics Specialist Conference*, April 17–20, 1967, New Orleans, LA, USA, pp. 65–89
[8] Torrance K E and Sparrow E M 1967 *J. Opt. Soc. Am.* **57** 1105
[9] Zha Z W, Zhu J Y, Yang X F, Huang X, Guo H X, Xie A, Lu X J and Fu Z W 2022 *Proceedings of 23rd International Conference on Electronic Packaging Technology*, August 10–13, 2022, Dalian, China, pp. 1–5
[10] He Y, Wang D Z, Yin Q Y, Gao Y Y and Zheng L B 2022 *Proceedings of 23rd International Conference on Electronic Packaging Technology*, August 10-13, 2022, Dalian, China, pp. 1–6
[11] Farbaniec L and Eakins D E 2023 *Rev. Sci. Instrum.* **94** 034902
[12] Alajlouni S, Maize K and Shakouri A 2022 *Proceedings of 21st IEEE Intersociety Conference on Thermal and Thermomechanical Phenomena in Electronic Systems,* May 31–June 03, 2022, San Diego, CA, USA, pp. 1–10
[13] Wang M 2020 *Research on temperature measurement method based on visible image and machine learning*, M.S. Thesis (Wuhan: Huazhong University of Science and Technology) (in Chinese)
[14] Du W J, Ye Q Z, Yuan Z and Li C M 2022 *High Voltage Electronics* **58** 221 (in Chinese)
[15] Nie X F, Ye Q Z, Yuan Z and Han M T 2021 *Proceedings of the 16th Annual Conference of China Electrotechnical Society*, September 24–26, 2021, Springer, Singapore, pp. 616–627
[16] Yang J F, Qiao P R, Li Y M and Wang N 2019 *Statistics and Decision Making* **35** 36 (in Chinese)
[17] Yu K, Jia L, Chen Y Q and Xu W 2013 *Proceedings of CCF Conference on Artificial Intelligence*, July 31–August 2, 2013, Beijing,China, pp.65-89
[18] Zheng Y P, Li G Y and Li Y 2019 *Computer Engineering and Applications* **55** 12 (in Chinese)
[19] Li J, Yang L Z, Ding W, Mao X Z, Fan J J, Wang J F, Shang H F and Ti G 2021 *Appl. Opt.* **60** 4004
[20] Lai X L, Li Q Y, Wu X Y, Liu G D, Chen Z Y and Pu J X 2021 *IEEE Access* **9** 68387
[21] Fan W R, Chen T R, Xu X Q, Chen Z Y, Hu H Z, Zhang D L, Wang D W, Pu J X and Zhu S Y 2022 *Laser & Photonics Reviews* **16** 2100719